

Coherent transport and manipulation of spins in indirect exciton nanostructures

A. Violante,^{1,*} R. Hey,¹ and P. V. Santos¹

¹*Paul-Drude-Institut für Festkörperelektronik, Hausvogteiplatz 5-7, 10117 Berlin, Germany*

(Dated: August 13, 2018)

We report on the coherent control and transport of indirect exciton (IX) spins in GaAs double quantum well (DQW) nanostructures. The spin dynamics was investigated by optically generating spins using a focused, circularly polarized light spot and by probing their spatial distribution using spatially and polarization resolved photoluminescence spectroscopy. Optically injected exciton spins precess while diffusing over distances exceeding $20\ \mu\text{m}$ from the excitation spot with a spatial precession frequency that depends on the spin transport direction as well as on the bias applied across the DQW structure. This behavior is attributed to the spin precession in the effective magnetic field induced by the spin-orbit interaction. From the dependence of the spin dynamics on the transport direction, bias and external magnetic fields we directly determined the Dresselhaus and Rashba spin splitting coefficients for the structure. The precession dynamics is essentially independent on the IX density, thus indicating that the long spin lifetimes are not associated with IX collective effects. The latter, together with the negligible contribution of holes to the spin dynamics, are rather attributed to spatial separation of the electron and hole wave functions by the electric field, which reduces the electron-hole exchange interaction. Coherent spin precession over long transport distances as well as the control of the spin vector using electric and magnetic field open the way for the application of IX spins in the quantum information processing.

PACS numbers: 71.35.-y, 75.76.+j, 75.70.Tj, 73.21.Fg

I. INTRODUCTION

An indirect (or dipolar) exciton (IX) consists of a Coulomb-correlated electron-hole pair with the individual particles confined in two closely spaced quantum wells (QWs) in a double quantum well (DQW) structure (cf. Fig. 1) subjected to a transverse electric field F_z . F_z controls via the quantum confined Stark effect both the IX energy and radiative lifetime, which can reach the ms-range.¹ The electric field can be used to laterally confine IX gases in DQW plane using electrostatic gates² as well as to control the interconversion between IX and photons. In addition, the electrical dipoles arising from the charge separation give rise to strong repulsive exciton-exciton interactions³. Finally, IXs are composite bosons and, therefore, susceptible to the formation of collective exciton phases, as evidenced by the experiments presented in Refs. 4–6. These interesting IX properties have been combined to demonstrate different device functionalities including light storage cells, switches, and transistors^{7–9}. The long IX lifetimes also enable the long-range transport and coupling of IX packets. Different approaches have also been introduced for the transport of IXs based on bare diffusion,¹⁰ drift induced by repulsive IX-IX interactions,⁴ or by using spatially varying electric fields, including electrostatic ramps¹¹ as well as moving electrostatic¹² and acoustic lattices^{13–15}.

Recently, the confinement of single IXs has been demonstrated,² thus opening the way for applications of single IXs in quantum information.¹⁶ Here, the manipulation and transport of IX spins offers further exciting perspectives. IXs have several favorable properties for spin control and manipulation. The reduced overlap between the electron and hole wave functions reduces not

only the radiative lifetime but also the exchange interaction between the exciton-bound electron spins and the short-living hole spins (the excitonic or Bir-Aronov-Pikus (BAP) mechanism^{17,18}), thus enhancing the exciton spin lifetime.^{19–21}

The long lifetime also enables for spin control using the spin-orbit (SO) coupling. Due to the Bulk Inversion Asymmetry (BIA) intrinsic to the noncentrosymmetric III-V materials (such as GaAs),^{22,23} moving spins feel an effective magnetic field (the Dresselhaus field,²⁴ \mathbf{B}_D), which modifies the spin vector during precession. In addition, the Structural Inversion Anisotropy (SIA) created by F_z induces a tunable contribution to the SO magnetic field (the Rashba field,²⁵ \mathbf{B}_R), thus providing a powerful tool for the dynamic spin control during motion. F_z also affects spins by changing the g -factor.²⁶ The SO fields can, however, also lead to the dephasing of exciton spin ensembles (the D'yakonov-Perel' dephasing mechanism). The spin dephasing time can be electrically controlled by selecting F_z to modulate the total SO field $\mathbf{B}_{SO} = \mathbf{B}_D + \mathbf{B}_R$.²⁷ The IX spin lifetime also enhances under high particle densities. In analogy with the spin dynamics of atomic condensates,²⁸ the latter has been attributed to the formation of collective IX phases.^{5,20,29–31} In particular, experiments carried out in this regime have led to the observation of spin currents in IX gases with a variety of spatially resolved polarization patterns,^{31,32} which have been attributed to the SO magnetic field.

Most of the previous IX spin studies have addressed the spin dynamics very close to the spin excitation area (i.e., within distances $< 10\ \mu\text{m}$), one exception being the self-organized extended (i.e., $> 20\ \mu\text{m}$) spin patterns reported for the collective regime at high IX densities.⁵ In this work, we demonstrate that optically injected IX

spins can be transported over distances exceeding $20 \mu\text{m}$ from the injection spot. The spins coherently precess during motion: the spatial precession period depends on the motion direction and can be controlled by the vertical field F_z applied across the DQW. This precession behavior, which does not depend on IX density, is attributed to the precession of the electron spins in the anisotropic SO field. From the dependence of the spin polarization on F_z , motion direction, and external magnetic field \mathbf{B}_{ext} we have determined the IX spin lifetime as well as the absolute magnitude and orientation of the SO fields in the DQW structures. In contrast to the spin patterns in collective regime addressed in Ref.⁵, we show that transport and manipulation of IX ensembles reported here takes place in the drift-diffusive regime and can be potentially extended down to the single spin level.

In the following, we first describe the sample structure and the photoluminescence (PL) technique used to probe the transport of exciton spins. We then present experimental results demonstrating the transport and coherent precession of IX spins in the SO field together with detailed studies of the spin dynamics as a function of propagation direction, bias, and external magnetic fields. These results on spin transport and SO effects are compared to the state-of-the-art in the final sections of the manuscript.

II. EXPERIMENTAL DETAILS

The samples used in the experiment contain three sets of asymmetric GaAs DQWs grown by molecular beam epitaxy on a n^+ -doped GaAs(001) substrate [cf. Figs. 1(a)-(b)]. Each DQW is formed by a $d_{QW,1} = 14 \text{ nm}$ (QW₁) and a $d_{QW,2} = 17 \text{ nm}$ -thick QW (QW₂) separated by a thin (4 nm-thick) $Al_{0.3}Ga_{0.7}As$ barrier. Multiple DQWs were used in order to enhance the photon yield of the PL experiments. The different QW widths enable the selective generation of direct excitons in either QW₁ or QW₂ by the appropriate selection of the excitation wavelength³³. The electric field F_z for the formation of IX s was induced by a bias voltage V_{BIAS} applied between the n -doped substrate and a thin (10 nm-thick) semitransparent Ti electrode (STE) deposited on the sample surface.

The spectroscopic experiments were carried out in a He bath cryostat at 2 K. Excitons were generated using a right circularly polarized beam from a cw Ti:Sapphire laser resonant with the electron-heavy hole direct exciton (DX) transition of the wider (QW₂) QW. The laser was focused onto a spot with a diameter of $2.5 \mu\text{m}$ using a microscope objective. The PL around the laser spot was collected by the same objective, analyzed regarding the circular polarization, and then imaged on the entrance slit of a spectrometer connected to a cooled charge-coupled-device (CCD) camera. The detected CCD images contain information about the energy (direction perpendicular to the slit) and spatial distribution of the PL inten-

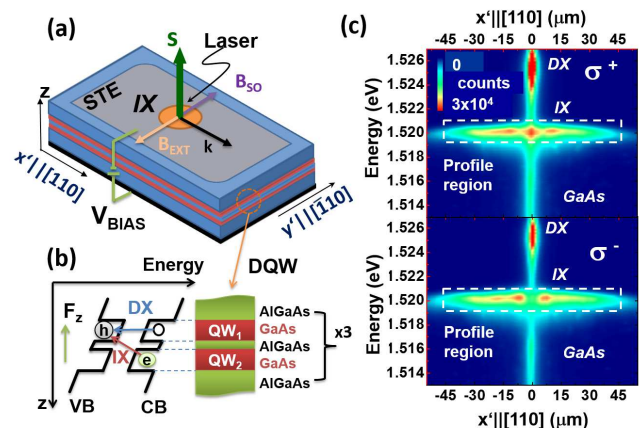


FIG. 1: (a) Double quantum well (DQW) structures for indirect exciton (IX) spin transport. The IX s are optically excited using a focused laser pulse in a DQW subject to an electric field (F_z) induced by a bias V_{BIAS} applied between the doped substrate and a semitransparent top electrode (STE). IX spin transport is mapped by imaging the IX photoluminescence (PL) emitted along direction k with polarization sensitivity. During motion along k , the spins precess under the spin-orbit (B_{SO}) and external magnetic field (B_{ext}). (b) Energy band diagram of the GaAs/(Al,Ga)As DQW along the vertical (z) direction showing the direct (DX) and IX transitions under the electric field F_z . (c) Spatially and spectrally resolved images of the PL with right (σ^+ , upper panel) and left (σ^- , lower panel) circular polarizations recorded under a bias $V_{\text{BIAS}} = -2 \text{ V}$ and a laser power of $13 \mu\text{W}$. DX and IX denote the emission from direct and indirect excitons in the DQW structure, while the line at 1.515 eV arises from excitons in the GaAs substrate.

sity (along the slit). The spatial (coordinate r) dependence of the spin polarization was calculated according to $\rho_z(r) = [I_{\sigma^+}(r) - I_{\sigma^-}(r)] / [I_{\sigma^+}(r) + I_{\sigma^-}(r)]$, where $I_{\sigma^+}(r)$ ($I_{\sigma^-}(r)$) denote the PL intensity at r with right (left) circular polarization.

III. RESULTS

A. Coherent spin precession during transport

Figure 1(c) compares PL images with right (σ^+) and left (σ^-) polarization recorded with the spectrometer slit aligned with the sample crystallographic direction $x' = [110]$. The emission patterns at 1.515 eV and 1.525 eV arise, respectively, from excitons in the GaAs substrate and from the low energy tail of DXs in QW₂. In both cases, the emission is restricted to a region close to the excitation spot, thus indicating negligible diffusion distances for these excitations. The line at 1.520 eV is associated with the emission of IX s in the DQW structure, which in this case was subject to a bias $V_{\text{BIAS}} = -2 \text{ V}$. The emission extends to radii exceeding $40 \mu\text{m}$ - these

long transport distances arise from the fact that the IXs are driven not only by diffusion but also by the drift forces induced by repulsive exciton-exciton dipolar interactions at the areas of high exciton density close to the excitation area. This assertion is supported by the strong dependence of the extension of the IX PL cloud on the excitation density P_l , as displayed by the dashed and dash-dotted lines in Fig. 2(a). These curves displayed the spatial dependence of the total PL intensity (i.e., $[I_{\sigma^+}(r) + I_{\sigma^-}(r)]$) determined from PL images for laser excitation powers of $P_l = 13 \mu\text{W}$ (as in Fig. 1(c)) and $1.6 \mu\text{W}$, respectively. The characteristic shape of the spatial PL profiles are consistent with the observations of Ref.⁴, which reported that the IX PL reduces in the area of hot IX close to the excitation spot. Furthermore, a closer look to Fig. 1(c) also reveals that the IX emission energy red-shifts as one moves away from the excitation spot. In fact, the average IX emission energy at $x' = 0 \mu\text{m}$ is $\sim 0.5 \text{ meV}$ higher than at $x' = 75 \mu\text{m}$. This energetic blue-shift is attributed to the strong repulsive IX-IX interaction at the high IX densities (estimated³⁴ to be of $2 \times 10^{10} \text{ cm}^{-2}$) close to $x' = 0$.

The intensity of the circularly polarized IX emission in Fig. 1(c) is also spatially modulated with the maxima for the σ^+ polarization corresponding to minima in the σ^- polarization. The symbols in Fig. 2(a) display the corresponding profiles for the spin polarization ρ_z . This spatial PL modulation is attributed to the precession of the IX electron spins in the effective SO magnetic field B_{SO} during their motion away from the excitation spot. The ρ_z oscillations extend over a range of radial distances shorter than the radius of the emission cloud. While the amplitude of the oscillations increases with P_l , their spatial period remains essentially constant. A similar increase in spin polarization with excitation density was previously reported in Ref.²⁰ and attributed to the onset of collective exciton effects. The fact that the spatial precession period does not change with the excitation density indicates, however, that the spin precession rates under the SO field does not depend on the IX density. In addition, the larger ρ_z amplitudes in our case is at least in part due to the shorter expansion times of the IX cloud resulting from IX-IX interactions under high P_l , which reduces the impact of spin scattering processes.

The solid lines in Fig. 2(a) are fits of the experimental results to damped oscillations with a spatial dependence given by:

$$\rho_s(\mathbf{r}) = \rho_s(0)e^{-r/\ell_s} \cos(2\pi r/\ell_p(\hat{\mathbf{r}})). \quad (1)$$

Here $\ell_p(\hat{\mathbf{r}})$ is the spin spatial precession period for propagation along $\hat{\mathbf{r}}$, which is equal to the SO precession period ℓ_{so} in the absence of external magnetic fields. ℓ_s denotes the effective spin transport decay length. Equation (1) describes the spin dynamics in a non-degenerate QW at low temperatures (i.e., for thermal energies less than the QW confinement energy), when spin precession rate $\Omega_{so}(\mathbf{k}) = \frac{\mu_B B_{SO}}{\hbar}$ becomes proportional to the elec-

tron wave vector \mathbf{k} . Under this condition, the spin precession period (for $\mathbf{B}_{\text{ext}} = 0$) $\ell_p = \ell_{so} = \frac{n_e}{2\pi\hbar^2} \frac{\hbar}{\Omega_{so}(\mathbf{k})}$ only depends on direction $\hat{\mathbf{r}}$. The spin decay length ℓ_s , in contrast, depends on temporal dynamics of the carrier motion as well as on the details of the spin scattering processes. The fits carried out with a single value for ℓ_p (i.e., independent of r) displayed in Eq. 1 reproduces very well the measured spin polarization profiles.

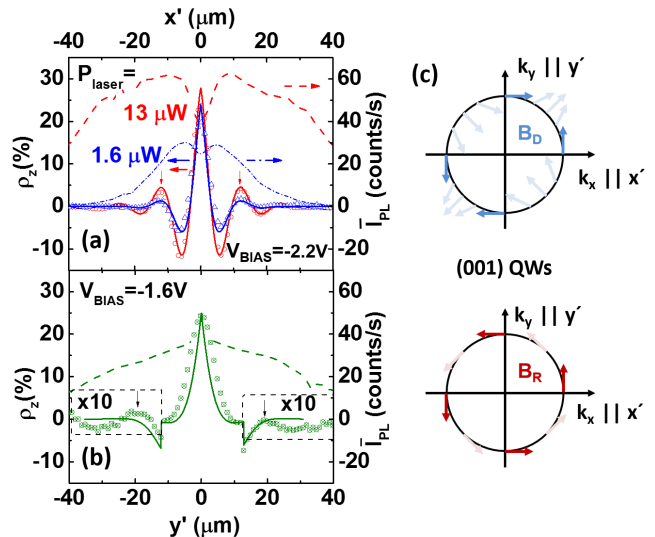


FIG. 2: (a) Profiles for the spin polarization (ρ_s , symbols) and for the average PL intensity (\bar{I}_{PL} , dashed and dot-dashed lines) for exciton transport along the $x' \parallel [110]$ (symbols) recorded for laser excitation densities $P_l = 1.6 \mu\text{W}$ (open symbols) and $13 \mu\text{W}$ (solid symbols). and $[\bar{1}10]$ directions (open symbols). (b) Corresponding profiles for transport along $y' \parallel [\bar{1}10]$ recorded for $P_l = 6 \mu\text{W}$. The solid lines superimposed on the symbols are fits of the experimental results to Eq. 1. (c) In-plane dependence of the Dresselhaus (B_D) and Rashba (B_R) contributions to the SO effective magnetic field $B_{SO} = B_D + B_R$.

B. Dependence on propagation direction

The wave vector (\mathbf{k}) dependence of the SO contributions $\mathbf{B}_D(\mathbf{k})$ and $\mathbf{B}_R(\mathbf{k})$ for a III-V QW is illustrated in Fig. 2(c). Here, we use a reference frame defined by the axes $x' \parallel [110]$, $y' \parallel [\bar{1}10]$, and $z \parallel [001]$. The associated (temporal) electron spin precession frequencies Ω_i , ($i = D, R$) can be written as a function of the wave vector \mathbf{k} as:³⁵

$$\hbar\Omega_D(\mathbf{k}) = \gamma \left(\frac{\pi}{d_{QW}^{\text{eff}}} \right)^2 \begin{bmatrix} k_{y'} \\ k_{x'} \\ 0 \end{bmatrix} \quad \text{and} \quad (2)$$

$$\hbar\Omega_{\mathbf{R}}(\mathbf{k}) = 2F_z r_{41} \begin{bmatrix} k_{y'} \\ -k_{x'} \\ 0 \end{bmatrix} \quad (3)$$

where γ and r_{41} are the Dresselhaus and Rashba spin constants, respectively. Equations 2 and 3 apply for small wave vectors (i.e., $|k'_{x'}|, |k'_{y'}| \ll \frac{\pi}{d_{\text{QW}}^{\text{eff}}}$). $d_{\text{QW}}^{\text{eff}}$ is the effective extension along z of the electronic wave function in the QW confining the electrons (QW₂ in the present case, as determined by the sign of V_{BIAS}). $d_{\text{QW}}^{\text{eff}}$ is determined by both the QW width and by the penetration depth into the barrier layers. The corresponding amplitudes of the spatial precession frequencies $\ell_{so,i}^{-1}$ can be derived from the precession distance required for a spin rotation by 2π . The following expressions are obtained:³⁶

$$\ell_{so,D}^{-1} = \gamma \frac{m_e}{2\pi\hbar^3} \left(\frac{\pi}{d_{\text{QW}}^{\text{eff}}} \right)^2 \quad \text{and} \quad \ell_{so,R}^{-1} = \frac{m_e}{\pi\hbar^3} r_{41} F_z. \quad (4)$$

If $\mathbf{B}_D \parallel \mathbf{B}_R$ the resulting spatial precession frequency will be given by $\ell_{so}^{-1} = |\ell_{so,D}^{-1} \pm \ell_{so,R}^{-1}|$, where the sign is defined by the relative orientation of the two fields.

Equations 2 and 4 predicts that the spatial precession period ℓ_{so} depends both on transport direction and on bias electric field F_z . In order to check the in-plane anisotropy of \mathbf{B}_{SO} , we show in Fig. 2(b) spin polarization profiles recorded for IX motion along the $[1\bar{1}0]$ surface direction (i.e., orthogonal to the one in Figs. 1(c) and 2(b)). The period of the precession oscillations is much larger than for the motion along the $[110]$ direction. The larger period, which in this case becomes comparable with the spin decay length, makes the amplitude of the oscillations weaker than in Fig. 2(a). The dependence of ℓ_{so} on transport direction is in agreement with the diagrams of Fig. 2(c): while \mathbf{B}_D and \mathbf{B}_R add for motion along $[110]$, they partially cancel each other for motion along $[\bar{1}10]$, thus leading to a weaker SO field. Interestingly, while a weaker \mathbf{B}_{SO} reduces spin scattering, it does not necessarily improve the visibility of the ρ_z oscillations since one also has to satisfy the constraint $\ell_{so} < \ell_s$. On the other hand, a stronger \mathbf{B}_{SO} reduces the spatial precession period. In this case, however, one needs to reduce the excitation spot to dimensions at least a factor of 2 smaller than the oscillation period in order to measure the oscillations.

C. Electric spin control

The electric control of the spin precession frequency is demonstrated by the series of profiles recorded for transport along $[110]$ in Fig. 3(a). The amplitude F_z of electric field was determined from the applied bias V_{BIAS} using the procedure described in Ref.¹⁴. The spatial precession period ℓ_{so} reduces by over 15% with increasing F_z ,

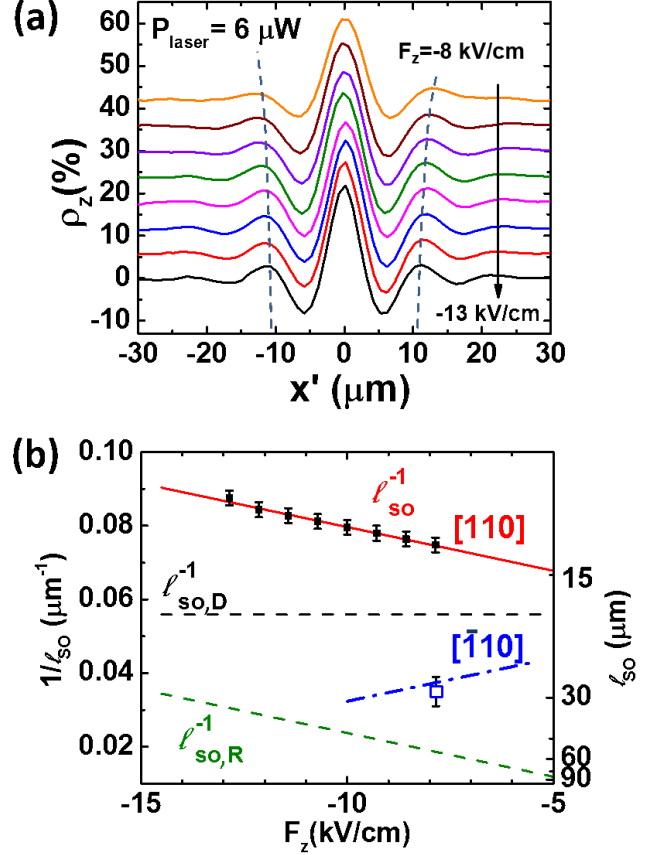


FIG. 3: (a) Profiles for the spin polarization (ρ_s , symbols) recorded for increasing electric fields F_z applied along the growth direction of the DQW structure. (b) Dependence of the spatial spin precession frequency $1/\ell_{so}$ on the electric field F_z for transport along $x' \parallel [110]$ (solid symbols) and $y' \parallel [\bar{1}10]$ (open symbol). The solid line is a fit of the data along $[110]$ to $\ell_{so}^{-1} = \ell_{so,D}^{-1} + \ell_{so,R}^{-1}$ (cf. Eq. 4) with $\gamma = 17.9 \text{ eV}\text{\AA}^3$, $r_{41} = -8.5 \text{ eV}\text{\AA}^2$, and $d_{\text{QW}}^{\text{eff}} = 21 \text{ nm}$. The corresponding inverse spatial precession periods $\ell_{so,D}^{-1}$ and $\ell_{so,R}^{-1}$ are illustrated by the dashed lines. The dot-dashed line shows the expected inverse precession period for motion along $[\bar{1}10]$.

thus indicating an enhancement of the Rashba field \mathbf{B}_R as well as of the total SO field \mathbf{B}_{SO} . Larger changes can be in principle be achieved by increasing the bias across the DQWs. These, however, also reduce the PL yield and may lead to field-induced carrier leakage out of the DQW structure, thus hampering an efficient spin detection.³⁷

The measured spatial precession frequencies (ℓ_{so}^{-1}) are plotted as a function of the transverse electric field in Fig. 3(b). The solid line is a fit of the data measured along $[110]$ to the expression: $\ell_{so}^{-1} = \ell_{so,D}^{-1} + \ell_{so,R}^{-1}$ (cf. Eq. 4), which gives $\gamma = 17.9 \text{ eV}\text{\AA}^3$, $r_{41} = -8.5 \text{ eV}\text{\AA}^2$, and $d_{\text{QW}}^{\text{eff}} = 21 \text{ nm}$ (the signs for γ and r_{41} will be determined below). The corresponding inverse precession periods $\ell_{so,D}^{-1}$ and $\ell_{so,R}^{-1}$ for propagation along this direc-

tion are illustrated by the dashed lines. For the applied bias, indirect excitons are created in the DQW structure with the electrons confined within the wider (17 nm wide) QW. The value for $d_{\text{QW}}^{\text{eff}}$ used in the fits is compatible with an electronic wave function with a penetration depth of 2 nm in the barriers. As will be further discussed later, these SO parameters agree well with values reported in the literature.

The open symbol in Fig. 3(b) shows the inverse precession period measured for spin propagation along y' , where the Dresselhaus contribution changes in sign relative to the x' . The measured value agrees well with the calculated inverse periods ℓ_{so}^{-1} for this propagation along this direction (dash-dotted line). Note that the change in relative signs of the Rashba and Dresselhaus effective magnetic fields can in principle also be attained for a fixed motion direction by simply reversing the bias polarity. For the asymmetric DQWs used in the present experiments, however, a reversal in direction of F_z moves the electrons to the narrow QW, thus also changing the magnitude of the Dresselhaus contribution. In addition, while the leakage current is very low for negative biases (a few nA), it increases considerably for high positive biases, thus indicating enhanced carrier leakage.

D. Magnetic field dependence

An external magnetic field \mathbf{B}_{ext} applied along the DQW plane provides an additional degree of freedom to control the spin vector. The experiments were carried out under the configuration illustrated in Fig. 1(a), where one maps the spins moving along x' under an external field $\mathbf{B}_{\text{ext}} \parallel \mathbf{y}'$ and collinear with \mathbf{B}_{so} . Figure 4(a) displays ρ_z profiles along x' recorded under different external magnetic fields. Large magnetic fields ($|\mathbf{B}_{\text{ext}}| > 6$ mT) mainly induce a reduction of the overall spin polarization (Hanle effect), from which one can extract the spin dephasing time τ_s . For that purpose, we plot in Fig. 4(b) the spin IX polarization at the excitation spot $\bar{\rho}_z$ as a function of \mathbf{B}_{ext} . The lines superimposed on the data points are fits to the Hanle expression:

$$\bar{\rho}_z(B_{\text{ext}}) = \frac{\bar{\rho}_z(0)}{1 + (\omega_L \tau_*)^2} \quad \text{with} \quad \hbar\omega_L = g_e \mu_B B_{\text{ext}}. \quad (5)$$

where $\bar{\rho}_z$ is the degree of polarization at the generation point, $\frac{1}{\tau_*} = \frac{1}{\tau_{IX}} + \frac{1}{\tau_s}$ with τ_{IX} the indirect exciton lifetime. By using the conduction band g-factor $|g_e| = 0.44$ and considering $\tau_{IX} \gg \tau_s$, one extracts from the fits spin lifetimes of 3 and 6 ns for excitation powers of $P_l = 1 \mu\text{W}$ and $13 \mu\text{W}$, respectively. These lifetimes are considerably longer than the typical carrier scattering times, thus indicating that the spin dynamics observed here takes place in diffusive (or strong scattering) regime.

Weak magnetic fields, in contrast, mainly affect the spin spatial precession frequency, as indicated by the symbols in Fig. 4(c). In contrast to the SO field, which

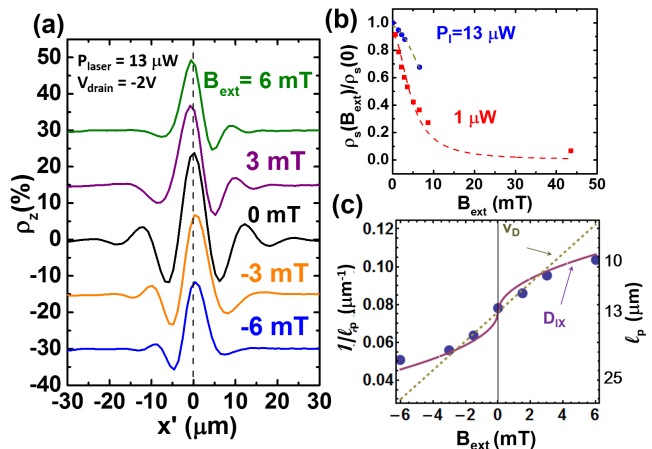


FIG. 4: (a) Spin polarization profiles as a function of an external magnetic field (B_{ext}). The curves are stacked for clarity. (b) ρ_z close to the excitation spot as a function of B_{ext} measured for optical excitation densities $P_l = 13 \mu\text{W}$ (squares) and $1 \mu\text{W}$ (dots). The dashed lines display fits to Eq. 5, from which one extracts spin lifetimes of 6 and 3 ns, respectively. (c) Dependence of the inverse precession period ($1/\ell_p = 1/\ell_{\text{so}} + 1/\ell_B$, where ℓ_{so} and ℓ_B are the precession period around the SO and external fields, respectively) on B_{ext} (symbols). The lines are the predictions from the diffusion (D_{IX}) and drift (v_D) models discussed in the text.

reverses with carrier momentum, the external field has a fixed direction and its action on the spin vector only depends on time. These features can be exploited to determine the absolute orientation of \mathbf{B}_{so} . When \mathbf{B}_{ext} is oriented along $+y'$ (upper curves for $\mathbf{B}_{\text{ext}} > 0$ in Fig. 4(a)), the spatial spin precession rate increases (reduces) for spins moving along $+x'$ ($-x'$). The opposite behavior is observed when the orientation of \mathbf{B}_{ext} reverses (curves for $\mathbf{B}_{\text{ext}} < 0$). From these results, together with the increase of the spatial precession frequency along the x' with $|F_z|$ (cf. Fig. 3(a), we unambiguously establish that both the Rashba and Dresselhaus spin orbit fields point towards y' when spins move along x' . The Dresselhaus splitting constant γ in Eq. 2 is thus positive while the Rashba parameter r_{14} is negative.

The different natures of the two fields allows us to extract information about the precession dynamics during motion and their impact on the precession period ℓ_p . Here, we first note that the different ℓ_p values in Fig. 4(a) along $+x'$ and $-x'$ implies that both fields (i.e., \mathbf{B}_{so} and \mathbf{B}_{ext}) must act simultaneously on the spins during the motion. This becomes clear if one considers the hypothetical situation, where the spins initially move to the final position x' within a very short time (thereby precessing only around $\mathbf{B}_{\text{so}}(\mathbf{k})$) and then remain trapped there until recombination (thus precessing only around \mathbf{B}_{ext}). In this case, \mathbf{B}_{ext} would simply add a fixed (i.e., position independent) phase to the spatial oscillations

determined by \mathbf{B}_{so} and ℓ_p would be the same for spin motion along both the positive and negative x' axes, in contrast to the results displayed in Fig. 4(a).

Since \mathbf{B}_{ext} and \mathbf{B}_{so} are collinear in Fig. 4(a), the inverse precession period can be written as $\ell_p^{-1} = \ell_{\text{so}}^{-1} + \ell_B^{-1}(\mathbf{B}_{\text{ext}})$, where $\ell_B^{-1}(\mathbf{B}_{\text{ext}})$ is the contribution associated with the external field. In order to account for the dependence of ℓ_p^{-1} on \mathbf{B}_{ext} one needs information about the spin position x' as a function of time (t). We consider the following two extreme situations. First, if the motion is mainly driven by the IX-IX repulsion forces at the excitation region, the carriers are expected to move with an approximately constant velocity v_D , yielding $\ell_B^{-1}(\mathbf{B}_{\text{ext}}) = \ell_{B,v_D}^{-1} = \frac{g\mu_B}{2\pi\hbar} \frac{\mathbf{B}_{\text{ext}}}{v_D}$. This model predicts the linear dependence of ℓ_p^{-1} on field indicated by the dashed line in Fig. 4(c). The very small values used for $v_D = 80$ m/s, which corresponds to only $\sim 1\%$ of the average exciton thermal velocity at 2 K, probably arise from the fact that diffusion has been completely neglected. While the behavior for small fields is well accounted for, the model fails to reproduce the deviations from linearity observed as the $|\mathbf{B}_{\text{ext}}|$ increases. The second extreme situation occurs if motion is purely driven by diffusion, in which case $x' = \sqrt{D_{IX}t}$, where D_{IX} is the IX diffusion coefficient. A straight-forward calculation yields $\ell_B^{-1}(\mathbf{B}_{\text{ext}}) = \ell_{B,D}^{-1} = \sqrt{\frac{g\mu_B}{2\pi\hbar} \frac{\mathbf{B}_{\text{ext}}}{D_{IX}}}$, leading to the behavior depicted by the solid line in Fig. 4(c). The calculations were carried out using an exciton diffusion coefficient $D_{IX} = 40 \times 10^{-4}$ cm²/s, which is approximately a factor of 2 larger than the one expected from Ref.¹⁰ for diffusion in a 15 nm wide QW. Despite its simplicity, this approximation reproduces reasonably well the measured behavior for large field amplitudes. A good fit requires, however, values for D_{IX} higher than those expected from Ref.¹⁰. This becomes necessary to reduce the IX transport (and precession) time and, in that way, compensate for the errors arising neglecting of drift effects. A more precise description of the spin dynamics by taking into account drift and diffusion is presently under study.

IV. DISCUSSIONS

The experimental results of the previous section unambiguously show the coherent precession of optically excited spins in the effective magnetic field \mathbf{B}_{so} induced by the SO interaction. The spin precession period depends on the in-plane motion direction - it is essentially independent of the IX density and can be controlled by external electric and magnetic fields. The measured spin lifetimes (of a few ns) indicate that transport takes place in the drift-diffusive regime. The spin dynamics is well-described by taking into account the SO parameters as well as the g-factor for electrons, thus showing that it is determined by the IX electron spins. In fact, the SO parameter $\gamma = 17.9$ eVÅ³ compares well with those determined from electron spin transport in (100),³⁸ (110),³⁹

and (111) QWs³⁷ with comparable widths. The magnitude of the Rashba parameter $r_{41} = -8.5$ eVÅ², however, lies above the experimental values of 4 and 6 ± 1 eVÅ² of Refs.⁴⁰ and³⁷, respectively, as well as the calculated value of 5.2 ± 1 eVÅ² from Ref.³⁶. While further investigations are required to clarify this difference, we speculate that it may be related to the asymmetric barriers in the DQW structure, which make the electronic wave function more susceptible to the applied electric fields.

The coherent transport and precession of electron spins in the SO field in the drift-diffusive transport regime has been previously reported for bulk GaAs layers^{41,42} as well as QW structures.^{38,39,41,43,44} In these experiments, electron transport has been driven by an external electric (or piezoelectric field): in this way, the spins could be moved over microscopic distances before dephasing (assumed to be due to the D'yakonov-Perel' mechanism⁴⁵) sets in. To our knowledge, however, the coherent precession of spins injected in an undoped QWs in the absence of an electric driving field demonstrated here has so far not been reported.

The observation of coherent spin precession in the SO field requires small ratios ℓ_{so}/ℓ_s (cf. Eq. 1). Here, $\ell_{\text{so}} \sim a_{\text{so}} \langle \Omega_{\text{so}} \rangle$ (a_{so} is a proportionality constant and the $\langle \rangle$'s denote thermal averages over the transport path) only depends on the strength of the SO interaction. The spin decay length ℓ_s , in contrast, depends on transport time. For purely diffusive motion in the D'yakonov-Perel' regime, $\ell_s \sim \frac{D_{IX}}{2r} \frac{1}{\tau_c \langle \Omega_{\text{so}}^2 \rangle}$, where τ_c is the carrier scattering time and D_{IX} the diffusion coefficient, reduces with transport distance r . As a result, the requirement $\ell_{\text{so}}/\ell_s \sim \frac{2\tau_c}{D_{IX}} \frac{\langle \Omega_{\text{so}} \rangle}{\langle \Omega_{\text{so}}^2 \rangle} a_{\text{so}} r < 1$ becomes increasingly difficult to be satisfied for long transport distances r (as well as for strong SO fields). In the present experiments, the expansion forces due to IX-IX repulsive interactions appear to have a fundamental role, since they considerably reduce the transport time, thus increasing ℓ_s and enabling the observation of precession oscillations.

Coherent spin patterns resulting from precession in the SO field have been reported for macroscopically ordered IX phases.^{5,31} The long spin coherence lengths required for their formation have been attributed to the reduced scattering in the ordered state, which enables the exciton transport in the ballistic regime. The results presented in the previous section show that long spin lifetimes and transport lengths, as well as coherent precession in the SO field can also be achieved in the drift-diffusive regime. This behavior is followed occurs over a wide range of exciton densities, thus indicating that it is not associated with collective effects. Interestingly, the spatial extent of the precession oscillations reported here is comparable to the ones for the self-organized spin patterns.³¹ There are additional fundamental differences between the two cases. While the spin pattern observed in Ref.³¹ results from self-organization and does not rely on the initial exciton polarization, the ones presented here appear as a consequence of the coherent transport of optically injected spins. In addition, the dynamics observed here is

associated with electron spin precession, while Ref.³¹ has invoked the simultaneous evolution of hole and electron spins.

Finally, as in most of the reports of coherent precession of optically injected spins in the SO field, the absence of hole spin contributions to the spin dynamics is attributed to the short hole spin coherence times as well as the spatial separation of the electron and hole wave function in the DQW structure. Since we have excited and probed *IX* spins, an interesting question is whether the electrons and hole remain bound during transport. Although we cannot present a conclusive evidence for this behavior, we mention that the *IX* spins have been excited with small excess energy (approx. 10 meV), thus reducing the probability of exciton dissociation followed by the spatial separation of electrons and holes. In addition, the *IX* spatial profiles (cf., e.g., Fig. 1(c)) do not show the characteristic rings observed when electrons and holes diffuse independently.

V. CONCLUSIONS

We have presented experimental evidence for the coherent precession of exciton spins during transport in the effective magnetic field induced by the SO interaction. The precession dynamics is essentially independent of the *IX* density, but can be controlled by an external bias (via changes in the SO field) or magnetic field. The

spin dynamics are well explained by taking into account electron spin precession, with no noticeable hole spin contribution. The technique used by us allows for the control and discrimination of precession effects arising from the Rashba and Dresselhaus SO contributions, as well as those induced by an external magnetic field. In this way, we were able to directly determine the absolute value and sign of the spin splitting parameters for the Rashba and Dresselhaus SO mechanisms. In addition, the spin dynamics in the presence of an external magnetic field yield information about the precession dynamics during transport. The long spin transport distances as well as the control of the spin vector open the way for the use of *IX* spins to encode and manipulate quantum information in opto-electronic semiconductor devices.

VI. ACKNOWLEDGEMENTS

We thank Manfred Ramsteiner for discussions and comments on the manuscript. We are indebted to S. Rauwerdink, W. Seidel, S. Krauß, and A. Tahraoui for the assistance in the preparation of the samples. We also acknowledge financial support from the German DFG (grant SA-598/9).

* e-mail address: violante@pdi-berlin.de

¹ K. Sivalertporn, L. Mouchliadis, A. L. Ivanov, R. Philp, and E. A. Muljarov. Direct and indirect excitons in semiconductor coupled quantum wells in an applied electric field. *Phys. Rev. B*, 85:045207, Jan 2012.

² G. J. Schinner, J. Repp, E. Schubert, A. K. Rai, D. Reuter, A. D. Wieck, A. O. Govorov, A. W. Holleitner, and J. P. Kotthaus. Confinement and interaction of single indirect excitons in a voltage-controlled trap formed inside double InGaAs quantum wells. *Phys. Rev. Lett.*, 110:127403, Mar 2013.

³ Kobi Cohen, Ronen Rapaport, and Paulo V. Santos. Remote dipolar interactions for objective density calibration and flow control of excitonic fluids. *Phys. Rev. Lett.*, 106(12):126402, Mar 2011.

⁴ L. V. Butov, A. C. Gossard, and D. S. Chemla. Macroscopically ordered state in an exciton system. *Nature*, 418:751, 2002.

⁵ A. A. High, J. R. Leonard, A. T. Hammack, M. M. Fogler, L. V. Butov, A. V. Kavokin, K. L. Campman, and A. C. Gossard. Spontaneous coherence in a cold exciton gas. *Nature*, 483:584, March 2012.

⁶ Yehiel Shilo, Kobi Cohen, Boris Laikhtman, Ken West, Loren Pfeiffer, and Ronen Rapaport. Particle correlations and evidence for dark state condensation in a cold dipolar exciton fluid. *Nature Communications*, 4:2335, 2013.

⁷ Alex A. High, Ekaterina E. Novitskaya, Leonid V. Butov, Micah Hanson, and Arthur C. Gossard. Control of exciton

fluxes in an excitonic integrated circuit. *Science*, 321:229, 2008.

⁸ Alexander G. Winbow, Aaron T. Hammack, Leonid V. Butov, and Arthur C. Gossard. Photon storage with nanosecond switching in coupled quantum well nanostructures. *Nano Lett.*, 7(5):1349–1351, 2007.

⁹ G. Grosso, J. Graves, A. T. Hammack, A. High, L. V. Butov, M. Hanson, and A. C. Gossard. Excitonic switches operating at around 100 k. *Nat. Photonics*, 3(10):577–580, October 2009.

¹⁰ Z. Vörös, R. Balili, D.W. Snoke, L. Pfeiffer, and K. West. Long-distance diffusion of excitons in double quantumwell structures. *Phys. Rev. Lett.*, 94:226401, 2005.

¹¹ A. Gärtner, A. W. Holleitner, J. P. Kotthaus, and D. Schuh. Drift mobility of long-living excitons in coupled GaAs quantum wells. *Appl. Phys. Lett.*, 89:052108, 2006.

¹² A. G. Winbow, J. R. Leonard, M. Remeika, Y. Y. Kuznetsova, A. A. High, A. T. Hammack, L. V. Butov, J. Wilkes, A. A. Guenther, A. L. Ivanov, M. Hanson, and A. C. Gossard. Electrostatic conveyer for excitons. *Phys. Rev. Lett.*, 106:196806, 2011.

¹³ J. Rudolph, R. Hey, and P. V. Santos. Long-range exciton transport by dynamic strain fields in a GaAs quantum well. *Phys. Rev. Lett.*, 99:047602, 2007.

¹⁴ S. S. Lazić, A. Violante, K. Cohen, R. Hey, R. Rapaport, and P. V. Santos. Scalable interconnections for remote indirect exciton systems based on acoustic transport. *Phys.*

- Rev. B, 89:085313, Feb 2014.
- 15 A. Violante, K. Cohen, S. Lazić, R. Hey, R. Rapaport, and P. V. Santos. Indirect exciton dynamics in moving potentials. New J. Phys., 89:085313, 2014.
 - 16 I. Zutic, J. Fabian, and S. D. Sarma. Spintronics: Fundamentals and applications. Rev. Mod. Phys., 76:323, 2004.
 - 17 A.G. Aronov G.L. Bir and G.E. Pikus. Sov. Phys. JETP, 42:705, 1975.
 - 18 G. L. Bir and G. E. Pikus. Symmetry and Strain-Induced Effects in Semiconductors. John Wiley & Sons, New York, 1974.
 - 19 AV Larionov, VB Timofeev, J Hvam, and C Soerensen. Collective behavior of interwell excitons in gaas/algaas double quantum wells. JETP Lett., 71(3):117–122, 2000.
 - 20 A. V. Larionov, V. E. Bisti, M. Bayer, J. Hvam, and K. Soerensen. Coherent spin dynamics of an interwell excitons gas in gaas/algaas coupled quantum wells. Phys. Rev. B, 73:235329, 2006.
 - 21 K. Kowalik-Seidl, X. P. Vögele, B. N. Rimpfl, S. Manus, J. P. Kotthaus, D. Schuh, W. Wegscheider, and A. W. Holleitner. Long exciton spin relaxation in coupled quantum wells. Appl. Phys. Lett., 97(1):011104, 2010.
 - 22 M. I. D'yakonov and V. I. Perel'. Spin orientation of electrons associated with the interband absorption of light in semiconductors. SPJETP, 33:1053–1059, 1971.
 - 23 Mikhail I. Dyakonov. Spin physics in semiconductors. Springer, 2008.
 - 24 G. Dresselhaus. Spin-orbit coupling effects in zinc blende structures. Phys. Rev., 100:580–586, Oct 1955.
 - 25 E. I. Rashba. Sov. Phys. Solid State, 2:1109, 1960.
 - 26 M. Poggio, G. M. Steeves, R. C. Myers, N. P. Stern, A. C. Gossard, and D. D. Awschalom. Spin transfer and coherence in coupled quantum wells. Phys. Rev. B, 70:121305(R), 2004.
 - 27 A.V. Larionov and L.E. Golub. Electric field control of spin-orbit splittings in gaas/algaas coupled quantum wells. Phys. Rev. B, 78:033302, 2008.
 - 28 E. A. Burt, R. W. Ghrist, C. J. Myatt, M. J. Holland, E. A. Cornell, and C. E. Wieman. Coherence, correlations, and collisions: What one learns about bose-einstein condensates from their decay. Phys. Rev. Lett., 79:337–340, 1997.
 - 29 V. B. Timofeev, A. V. Larionov, M. Grassi Alessi, M. Capizzi, A. Frova, and J. M. Hvam. Charged excitonic complexes in gaas/al0.35ga0.65as p-i-n double quantum wells. Phys. Rev. B, 60:8897–8901, 1999.
 - 30 J. R. Leonard, Y. Y. Kuznetsova, Sen Yang, L. V. Butov, T. Ostatnick, A. Kavokin, and A. C. Gossard. Spin transport of excitons. Nano Lett., 9:4204–4208, 2009.
 - 31 A. A. High, A. T. Hammack, J. R. Leonard, Sen Yang, L. V. Butov, T. Ostatnický, M. Vladimirova, A. V. Kavokin, T. C. H. Liew, K. L. Campman, and A. C. Gossard. Spin currents in a coherent exciton gas. Phys. Rev. Lett., 110:246403, Jun 2013.
 - 32 A. V. Kavokin, M. Vladimirova, B. Jouault, T. C. H. Liew, J. R. Leonard, and L. V. Butov. Ballistic spin transport in exciton gases. Phys. Rev. B, 88:195309, Nov 2013.
 - 33 M. Stern, V. Garmider, E. Segre, M. Rappaport, V. Uman-sky, Y. Levinson, and I. Bar-Joseph. Photoluminescence ring formation in coupled quantum wells: Excitonic versus ambipolar diffusion. Phys. Rev. Lett., 101(25):257402, 2008.
 - 34 Christoph Schindler Roland Zimmermann. Excitonexciton interaction in coupled quantum wells. Solid State Commun., 144:395, 2007.
 - 35 A. Hernández-Mínguez, K. Biermann, R. Hey, and P. V. Santos. Spin transport and spin manipulation in (110) and (111) GaAs quantum wells. Phys. Status Solidi B, in print:–, 2013.
 - 36 R. Winkler. Spin-Orbit Coupling Effects in Two-Dimensional Electron and Hole Systems, volume 191. Springer, Berlin, 2003.
 - 37 A. Hernández-Mínguez, K. Biermann, R. Hey, and P.V. Santos. Electrical suppression of spin relaxation in GaAs(111)B quantum wells. Phys. Rev. Lett., 109:266602, 2012.
 - 38 James A. H. Stotz, Rudolf Hey, Paulo V. Santos, and K. H. Ploog. Coherent spin transport via dynamic quantum dots. Nat. Mater., 4:585, 2005.
 - 39 O. D. D. Couto, Jr., F. Iikawa, J. Rudolph, R. Hey, and P. V. Santos. Anisotropic spin transport in (110) GaAs quantum wells. Phys. Rev. Lett., 98:036603, 2007.
 - 40 P. S. Eldridge, W. J. H. Leyland, P. G. Lagoudakis, R. T. Harley, R. T. Phillips, R. Winkler, M. Henini, and D. Taylor. Rashba spin-splitting of electrons in asymmetric quantum wells. Phys. Rev. B, 82(4):045317, Jul 2010.
 - 41 Y. Kato, R. C. Myers, A. C. Gossard, and D. D. Awschalom. Coherent spin manipulation without magnetic fields in strained semiconductors. Nature, 427:50, 2004.
 - 42 M. Beck, C. Metzner, S. Malzer, and G. H. Doehler. Spin lifetimes and strain-controlled spin precession of drifting electrons in zinc blende type semiconductors. Europhys. Lett., 75:597, 2006.
 - 43 H. Sanada, T. Sogawa, H. Gotoh, K. Onomitsu, M. Kohda, J. Nitta, and P. V. Santos. Acoustically induced spin-orbit interactions revealed by two-dimensional imaging of spin transport in GaAs. Phys. Rev. Lett., 106(21):216602, May 2011.
 - 44 H. Sanada, Y. Kunihashi, H. Gotoh, K. Onomitsu, M. Kohda, J. Nitta, P. V. Santos, and T. Sogawa. Manipulation of mobile spin coherence using magnetic-field-free electron spin resonance. Nat. Phys., 9:280, March 2013.
 - 45 M. I. D'yakonov and V. I. Perel'. Spin relaxation of conduction electrons in noncentrosymmetric semiconductors. Sov. Phys. Solid State, 13:3023–3026, 1972.